

Document downloaded from:

<http://hdl.handle.net/10251/51552>

This paper must be cited as:

Vayá Pérez, I.; Andreu Ros, Ml.; Jiménez Molero, MC.; Miranda Alonso, MÁ. (2014). Photooxygenation mechanisms in naproxen-amino acid linked systems. *Photochemical & Photobiological Sciences Photochemical and Photobiological Sciences*. 13:224-230. doi:10.1039/c3pp50252j.



The final publication is available at

<http://dx.doi.org/10.1039/c3pp50252j>

Copyright Royal Society of Chemistry

Cite this: DOI: 10.1039/c0xx00000x

www.rsc.org/xxxxxx

ARTICLE TYPE

Photooxygenation Mechanisms in Naproxen-Amino Acid Linked Systems

Ignacio Vayá,^a Inmaculada Andreu,^b M. Consuelo Jiménez^{a,*} and Miguel A. Miranda^{a,*}

Received (in XXX, XXX) Xth XXXXXXXXXX 20XX, Accepted Xth XXXXXXXXXX 20XX

DOI: 10.1039/b000000x

The photooxygenation of model compounds containing the two enantiomers of naproxen (NPX) covalently linked to histidine (His), tryptophan (Trp) and tyrosine (Tyr) has been investigated by steady state irradiation, fluorescence spectroscopy and laser flash photolysis. The NPX-His systems presented the highest oxygen-mediated photoreactivity. Their fluorescence spectra matched that of isolated NPX and showed a clear quenching by oxygen, leading to a diminished production of the NPX triplet excited state ($^3\text{NPX}^*\text{-His}$). Analysis of the NPX-His and NPX-Trp photolysates by UPLC-MS-MS revealed in both cases formation of two photoproducts, arising from reaction of singlet oxygen ($^1\text{O}_2$) with the amino acid moiety. The most remarkable feature of NPX-Trp systems was a fast and stereoselective intramolecular fluorescence quenching, which prevented efficient formation of $^3\text{NPX}^*\text{-Trp}$, thus explaining their lower reactivity towards photooxygenation. Finally, the NPX-Tyr systems were nearly unreactive and exhibited photophysical properties essentially coincident with those of the parent NPX. Overall, these results point to a type II photooxygenation mechanism, triggered by generation of $^1\text{O}_2$ from the $^3\text{NPX}^*$ chromophore.

1. Introduction

The most mutagenic and carcinogenic component of solar radiation is UVB light, which is directly absorbed by biomolecules.^{1,2} In addition, photosensitised oxidation is in the origin of lipid, protein or nucleic acids damage upon UVA-Vis excitation. It can be mediated by a variety of chromophores (naphthalene, anthracene, etc.) and operates through a type I (radical) or a type II (singlet oxygen, $^1\text{O}_2$) mechanism.³⁻⁸

Proteins are major targets for photosensitised oxidation, which is associated with loss of activity, denaturation, amino acid oxidation, fragmentation, etc.⁹⁻¹¹ In this context, amino acid residues such as histidine (His), tryptophan (Trp) and tyrosine (Tyr) are among the most vulnerable protein building blocks.¹²⁻¹⁴ Thus, His reacts efficiently with $^1\text{O}_2$, whereas Tyr acts as a radical trap site, inducing a cascade of reactions ultimately leading to protein modifications. In the case of Trp, both singlet oxygen and radical mechanisms can be involved.^{15,16}

Nonsteroidal anti-inflammatory drugs (NSAIDs), specially those belonging to the 2-arylpropionic acid family, constitute typical examples of photosensitising drugs,¹⁷⁻¹⁹ which can induce oxidative damage to specific amino acids in proteins.²⁰ Naproxen (NPX) is a NSAID containing a naphthalene chromophore, whose photobehaviour has been characterised in some detail.^{18,21} Indeed, it has recently been demonstrated that intermolecular photosensitisation of Trp by NPX can occur through a combination of both type I and type II mechanisms.²²

The use of tailored, well-defined linked systems has proven to be an appropriate tool to investigate excited state interactions involving fundamental processes such as energy or electron transfer, exciplex formation, etc. In addition, these systems are convenient models for biologically relevant entities.²³⁻²⁸

With this background, we report here a thorough mechanistic study on the photooxygenation of a series of naproxen-amino acid linked systems (Chart 1). The study includes steady-state irradiation, fluorescence, laser flash photolysis (LFP) and product analysis by means of liquid chromatography coupled to tandem mass spectrometry (UPLC-MS-MS).

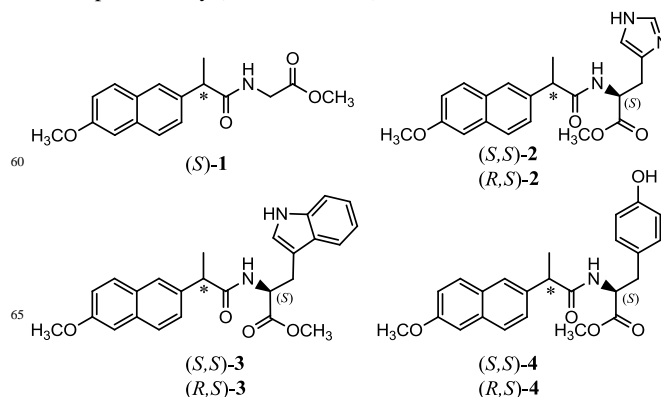


Chart 1 Chemical structure of the investigated naproxen-amino acid linked systems.

2. Experimental section

Materials and solvents. (*S*)- and (*R*)-NPX, (*S*)-Trp methyl ester hydrochloride, (*S*)-His methyl ester hydrochloride, (*S*)-Tyr methyl ester hydrochloride, glycine methyl ester hydrochloride, 1-(3-dimethylaminopropyl)-*N*-ethylcarbodiimide hydrochloride (EDC) and 1-hydroxybenzotriazole (BtOH) were commercially available. Reagent or spectroscopic grade solvents (hexane, ethyl acetate, acetonitrile) were used without further purification.

General. Steady state absorption spectra were recorded with a Perkin-Elmer Lambda 35 UV/Vis spectrophotometer. The ^1H NMR and ^{13}C NMR spectra were recorded in CDCl_3 or CD_3OD as solvent at 300 and 75 MHz, respectively, using a Varian Gemini instrument; chemical shifts are reported in δ (ppm). Combustion analyses were performed at the Instituto de Química Bio-Orgánica of the CSIC in Barcelona. The X-ray structures were determined at Unidade de Raios X, at the Universidade de Santiago de Compostela. Crystallographic data (excluding structure factors) for the structures of (*S,S*)-**2**, (*R,S*)-**2**, (*S,S*)-**3**, (*R,S*)-**3**, (*S,S*)-**4** and (*R,S*)-**4** have been deposited at the Cambridge Crystallographic Data Centre as supplementary publication numbers CCDC 662964, CCDC 662965, CCDC 662957, CCDC 662958, CCDC 662959 and CCDC 662960, respectively. Ultra Performance Liquid Chromatography (UPLC) was carried out on an ACQUITY UPLC system (Waters Corp.) with a conditioned autosampler at 4 °C. The separation was accomplished on an ACQUITY UPLC BEH C18 column (50 mm \times 2.1 mm i.d., 1.7 μm), which was maintained at 40 °C. The analysis was performed using acetonitrile and water (60 : 40 v/v containing 0.01% formic acid) as the mobile phase with a flow rate of 0.5 mL/min and an injection volume of 5 μL . The Waters ACQUITYTM XevoQToF Spectrometer (Waters Corp.) was connected to the UPLC system via an electrospray ionization interface. This source was operated in positive ionization mode at 100 °C with the capillary voltage at 1.5 kV and a temperature of desolvation of 300 °C. The cone and desolvation gas flows were 40 and 800 L/h, respectively. The collision gas flow and collision energy applied were 0.2 mL / min and 12 V, respectively. All data collected in Centroid mode were acquired using MasslynxTM software (Waters Corp.). Leucine-enkephalin was used at a concentration of 500 pg/ μL as the lock mass generating an $[\text{M}+\text{H}]^+$ ion (m/z 556.2771) and fragment at m/z 120.0813 with a flow rate of 50 $\mu\text{L}/\text{min}$ to ensure accuracy during the MS analysis.

Fluorescence measurements. Emission spectra were recorded on a JASCO spectrofluorometer system provided with a monochromator in the wavelength range 200-900 nm. The solutions were placed into 10 \times 10 mm² quartz cells with a septum cap and were purged with nitrogen or oxygen for at least 15 min before measurements. The absorbance of the samples at the excitation wavelength was kept below 0.1. Time-resolved measurements were performed with a Time Master fluorescence lifetime spectrometer (TM-2/2003) from PTI by means of the stroboscopic technique. All the experiments were carried out at room temperature (22 °C).

Laser flash photolysis experiments. The LFP experiments were performed by using a Brilliant Q-switched Nd:YAG laser (266 nm, 4 mJ per pulse, 5 ns fwhm) coupled to a Luzchem mLFP-111

miniaturized equipment. All transient spectra were recorded employing 10 \times 10 mm² quartz cells with 4 mL capacity and were bubbled during 15 min with N_2 or O_2 before acquisition. The absorbance of the samples was 0.2 at the laser excitation wavelength. All the experiments were carried out at room temperature.

Steady-state photolysis. Steady-state photolysis was performed by using a multilamp Luzchem photoreactor emitting at $\lambda_{\text{max}} = 300$ nm (14 \times 8 W lamps). Solutions (0.5 mg/mL) were irradiated for different times in acetonitrile, under N_2 , air or O_2 through quartz.

Analytical instrumentation. The irradiated solutions were analysed in an analytical Waters HPLC system connected to a PDA Waters 2996 detector, using an isocratic flux (0.7 mL/min) of MeCN/water/MeOH/HOAc (25:25:50:0.1 v/v/v/v) as eluent, and a C18 Kromasil 100 column, 5 μm (25 \times 0.4 cm).

Synthesis of the substrates. To a solution of 0.8 mmol of (*S*)- or (*R*)-NPX in acetonitrile (20 mL), 0.8 mmol of EDC and 0.8 mmol of BtOH were added as solids. The mixture was maintained under stirring, and then 0.8 mmol of the corresponding amino acid in 2 mL of acetonitrile were added dropwise. After three hours, the solvent was removed under vacuum; the crude solid was dissolved in methylene chloride, washed consecutively with diluted NaHCO_3 , 1 M HCl and brine. Final purification was performed by preparative layer chromatography on silica gel Merck 60 PF254, using hexane/ethyl acetate as eluent, followed by recrystallization.

N-[2-(*S*)-(6-Methoxy-2-naphthyl)propanoyl]glycine methyl ester. ^1H NMR (CDCl_3) δ : 7.75-7.70 (m, 3H), 7.41-7.39 (dd, $J_1 = 8.4$ Hz, $J_2 = 1.8$ Hz, 1H), 7.18-7.12 (m, 2H), 5.89 (m, 1H), 4.06-3.88 (m, 2H), 3.92 (s, 3H), 3.77 (q, 1H, $J = 7.2$ Hz), 3.70 (s, 3H), 1.62 (d, 3H, $J = 7.2$ Hz). ^{13}C NMR (CDCl_3) δ : 174.8, 170.6, 158.0, 136.2, 134.1, 129.5, 129.3, 127.9, 126.6, 126.5, 119.5, 105.9, 55.6, 52.6, 47.1, 41.6, 18.7. Anal. Calcd. for $\text{C}_{17}\text{H}_{19}\text{NO}_4$: C 72.54; H 6.09; N 6.51. Found: C 72.26; H 6.10; N 6.34.

N-[2-(*R*)-(6-Methoxy-2-naphthyl)propanoyl]glycine methyl ester. ^1H NMR (CDCl_3) δ : 7.75-7.70 (m, 3H), 7.41-7.39 (dd, $J_1 = 8.4$ Hz, $J_2 = 1.8$ Hz, 1H), 7.18-7.12 (m, 2H), 5.89 (m, 1H), 4.06-3.88 (m, 2H), 3.92 (s, 3H), 3.77 (q, 1H, $J = 7.2$ Hz), 3.70 (s, 3H), 1.62 (d, 3H, $J = 7.2$ Hz). ^{13}C NMR (CDCl_3) δ : 174.8, 170.6, 158.0, 136.2, 134.1, 129.5, 129.3, 127.9, 126.6, 126.5, 119.5, 105.9, 55.6, 52.6, 47.1, 41.6, 18.7. Anal. Calcd. for $\text{C}_{17}\text{H}_{19}\text{NO}_4$: C 72.54; H 6.09; N 6.51. Found: C 72.35; H 6.08; N 6.42.

N-[2-(*S*)-(6-Methoxy-2-naphthyl)propanoyl]-(*S*)-histidine methyl ester. ^1H NMR (CD_3OD) δ : 7.71-7.67 (m, 3H), 7.50 (br s, 1H), 7.38-7.35 (dd, $J_1 = 8.4$ Hz, $J_2 = 1.5$ Hz, 1H), 7.19 (d, $J = 2.4$ Hz, 1H), 7.12-7.08 (dd, $J_1 = 9.0$ Hz, $J_2 = 2.4$ Hz, 1H), 6.74 (br s, 1H), 4.66-4.61 (dd, $J_1 = 8.7$ Hz, $J_2 = 5.4$ Hz, 1H), 3.89 (s, 3H), 3.79 (q, $J = 7.2$ Hz, 1H), 3.59 (s, 3H), 3.12-3.06 (dd, $J_1 = 14.7$ Hz, $J_2 = 5.4$ Hz, 1H), 3.01-2.93 (dd, $J_1 = 14.7$ Hz, $J_2 = 8.7$ Hz, 1H), 1.45 (d, $J = 7.2$ Hz, 3H). ^{13}C NMR (CD_3OD) δ : 177.5, 173.7, 159.5, 138.0, 136.7, 135.6, 130.8, 130.6, 128.4, 127.8, 127.3, 120.2, 107.0, 56.1, 54.5, 53.0, 47.5, 30.3, 19.1. Anal. Calcd. for $\text{C}_{21}\text{H}_{23}\text{N}_3\text{O}_4$: C 66.13; H 6.08; N 11.02. Found: C 66.40; H 6.03; N 10.77.

N-[2-(*R*)-(6-Methoxy-2-naphthyl)propanoyl]-(*S*)-histidine methyl ester. ¹H NMR (CD₃OD) δ: 7.69-7.65 (d+d, *J* = 9.0 and 8.7 Hz, 2H), 7.61 (br s, 1H), 7.37 (br s, 1H), 7.30-7.26 (dd, *J*₁ = 8.7 Hz, *J*₂ = 1.8 Hz, 1H), 7.18 (d, *J* = 2.4 Hz, 1H), 7.12-7.08 (dd, *J*₁ = 9.0 Hz, *J*₂ = 2.4 Hz, 1H), 6.56 (br s, 1H), 4.66-4.62 (dd, *J*₁ = 8.7 Hz, *J*₂ = 5.4 Hz, 1H), 3.88 (s, 3H), 3.79 (q, *J* = 7.2 Hz, 1H), 3.69 (s, 3H), 3.08-3.02 (dd, *J*₁ = 14.7 Hz, *J*₂ = 5.4 Hz, 1H), 2.95-2.87 (dd, *J*₁ = 14.7 Hz, *J*₂ = 8.7 Hz, 1H), 1.48 (d, *J* = 7.2 Hz, 3H). ¹³C NMR (CD₃OD) δ: 177.5, 173.9, 159.5, 138.1, 136.5, 135.6, 130.8, 130.6, 128.5, 127.6, 127.2, 120.3, 107.0, 56.1, 54.4, 53.2, 47.4, 30.4, 18.9. Anal. Calcd. for C₂₁H₂₃N₃O₄: C 66.13; H 6.08; N 11.02. Found: C 66.18; H 6.27; N 10.77.

3. Results and discussion

3.1 Steady-state photolysis

Synthesis of compounds **1-4** (see chart 1) was performed by coupling of NPX with the appropriate amino acid methyl ester. They were fully characterised by spectroscopic techniques and X-ray diffraction (see Fig. 1 for the the (*S,S*)- diastereomers and Fig. S1 of ESI for the (*R,S*)- analogues). The glycine derivative (*S*)-**1** was selected as model system, since it contains the peptidic bond that could modulate the photoreactivity and the photophysical properties of the naphthalene moiety. Blocking the carboxy group of NPX in (*S*)-**1** was expected to avoid formation of photoproducts derived from decarboxylation of the parent drug.¹⁹

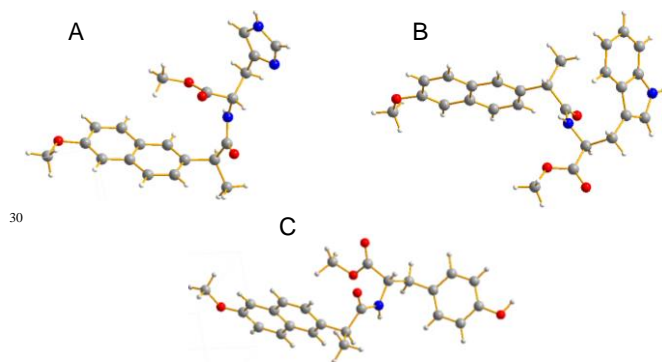


Fig. 1 X-ray structures of (*S,S*)-**2** (A), (*S,S*)-**3** (B) and (*S,S*)-**4** (C).

Irradiation was performed in a multilamp photoreactor (λ_{\max} = 300 nm, MeCN) under N₂, air or O₂ atmospheres. The course of photodegradation was followed by HPLC (detection at λ = 254 nm). As anticipated, the reference compound (*S*)-**1** was fairly photostable under all conditions (Fig. S2 of ESI). The same was true for the Tyr derivatives (*S,S*)- and (*R,S*)-**4**. By contrast, the behaviour of the histidine and tryptophan analogues exhibited different patterns (see Fig. 2 and Fig. S3 of ESI).

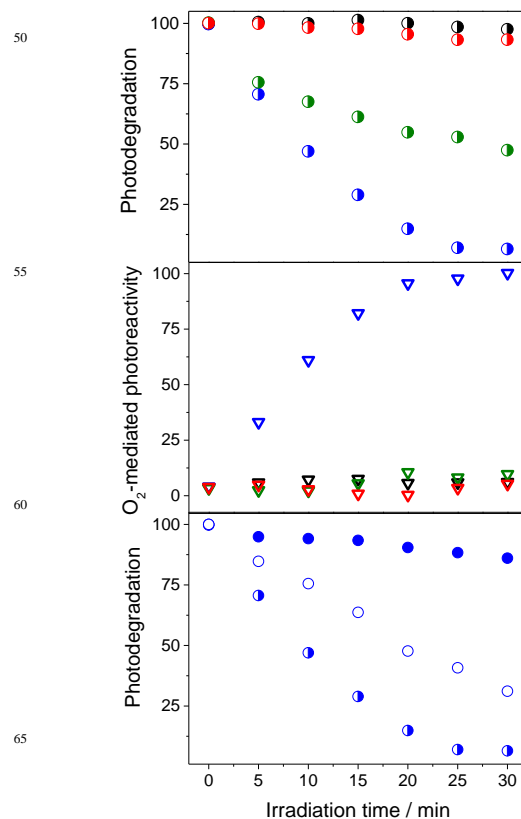


Fig. 2 Top: photoreactivity of (*S*)-**1** (black), (*S,S*)-**2** (blue), (*S,S*)-**3** (green) and (*S,S*)-**4** (red). Middle: oxygen-mediated photoreactivity of the same compounds (values under air minus values under nitrogen). Bottom: photoreactivity of (*S,S*)-**2** under different conditions. Codes: solid circles (N₂), half solid circles (air) and open circles (O₂).

Photodegradation of the investigated (*S,S*)- systems, under air, is shown in Fig. 2 (top). Clearly, the highest photoreactivity was observed for (*S,S*)-**2** followed by (*S,S*)-**3**. In order to clarify the role of oxygen in the overall photoreactivity, the extent of the photodegradation under nitrogen was subtracted from that obtained under air (Fig. 2 middle). Although this constitutes a simplified approach, it suggests that (*S,S*)-**2** is the substrate exhibiting the highest oxygen-mediated photoreactivity. In this context, the photobehaviour of (*S,S*)-**2** under N₂, air and O₂ atmospheres is compared in Fig. 2 (bottom). While photodegradation under N₂ was nearly negligible, this was not the case in oxygenated media. Interestingly, the photoreactivity in oxygen-saturated medium was lower than that observed for air-equilibrated solutions.

It is well known that photooxidation of His basically occurs through a type II mechanism, while Tyr mainly photoreacts through formation of radical intermediates.^{13,14,20,29,30} In addition, it has been previously demonstrated that NPX is able to photosensitise formation of ¹O₂ with a quantum yield ϕ_{Δ} = 0.27.³¹ This would be consistent with photodegradation of **2** in aerobic media and with the lack of reactivity of the Tyr analogues (Fig. S4 of ESI). Interestingly, although Trp can in principle be

photooxidised through both type I and type II mechanisms,^{9,22,32} a very low oxygen-mediated photoreactivity was noticed for **3** (Fig. 2, middle). In this context, to gain a better understanding of the involved photooxidation processes, photophysical studies by means of fluorescence and laser flash photolysis measurements were performed.

3.2 Photophysical studies

As stated above, the photoreactivity was found to be highly dependent on the presence of oxygen. Hence, the singlet and triplet excited state behaviour of the systems was investigated in the presence and absence of O₂.

The UV-vis absorption spectra of **1-4** were identical to the added spectra of isolated NPX and the corresponding amino acid subunits at the same concentration (Fig. S5 of ESI). This revealed the absence of any significant intramolecular ground-state interaction between the two moieties.

The emission spectra of (*S,S*)- and (*R,S*)-**2** were nearly identical to that of (*S*)-**1**, revealing the lack of quenching of the excited singlet state (¹NPX*) by His (Fig. S6 of ESI). However, a clear oxygen effect on the fluorescence intensity was observed (Fig. 3A). From the slope of the Stern-Volmer plot (Fig. 3A inset), taking into account the singlet lifetime ($\tau_F = 11.5$ ns), the quenching rate constant by oxygen was determined as $2.1 \times 10^{10} \text{ M}^{-1} \text{ s}^{-1}$ for (*S,S*)-**2**. This process competes with intersystem crossing, resulting in a diminished formation of the triplet excited state.

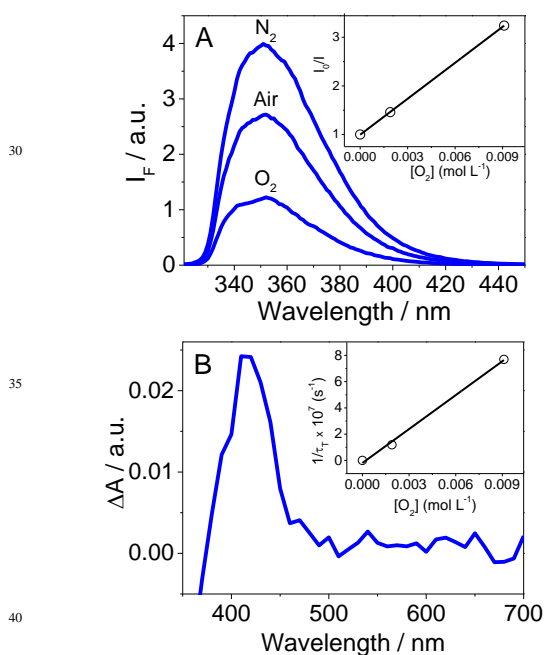


Fig. 3 A) Emission spectra of (*S,S*)-**2** ($\lambda_{\text{exc}} = 266$ nm, MeCN) in N₂, air or O₂. B) Transient absorption spectrum of (*S,S*)-**2** in MeCN/N₂ upon laser flash photolysis ($\lambda_{\text{exc}} = 266$ nm), obtained 2.9 μs after the laser pulse. Insets: Stern-Volmer plots for quenching of the singlet and triplet excited states by oxygen.

As regards the transient absorption experiments, (*S,S*)-**2**

displayed the typical naphthalene-like triplet-triplet absorption band corresponding to ³NPX* (Fig. 3B). The triplet lifetime (τ_T) was identical to that obtained for (*S*)-**1**, revealing the absence of any significant intramolecular interaction in the excited triplet state. From the Stern-Volmer plot for quenching by oxygen, shown in Fig. 3B inset, a rate constant value of $8.6 \times 10^9 \text{ M}^{-1} \text{ s}^{-1}$ was obtained.

Interestingly, photodegradation in saturated oxygen medium occurs to a lesser extent than in aerated solution (Fig. 2 bottom), where ¹O₂ is more efficiently formed as a combined result of poor quenching of the singlet and efficient quenching of the triplet excited states. A similar behaviour was observed for the (*R,S*)-analogue (Fig. S3 of ESI). The photophysical results are in agreement with a type II photooxidation mechanism for the O₂-mediated photoreactivity of NPX-His systems.

As regards the Trp and Tyr-based systems (**3** and **4**), their emission properties upon excitation at 266 nm (where both chromophores absorb) have been recently reported.²³ In the present work, fluorescence measurements have been performed at 310 nm, to achieve selective excitation of the NPX chromophore. In agreement with previous observations, a stereoselective charge transfer quenching was noticed for (*S,S*)- and (*R,S*)-**3**, whose fluorescence quantum yields were 0.09 and 0.04, respectively (compared to 0.45 for (*S*)-**1**).

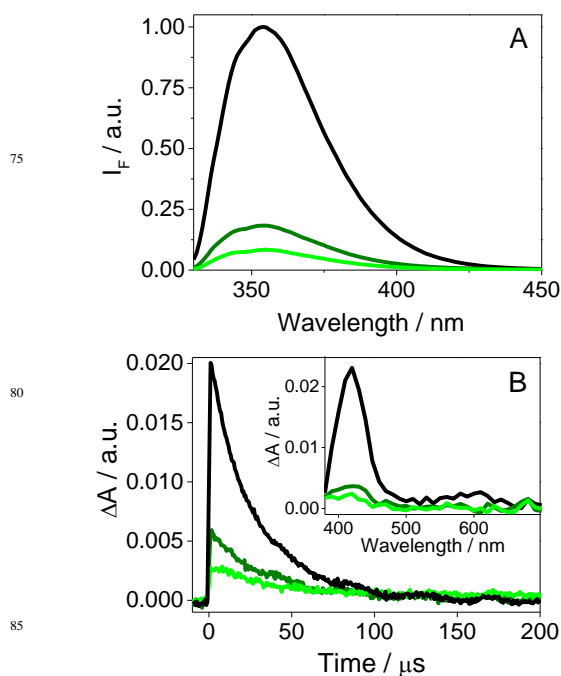


Fig. 4 Photophysical measurements on (*S*)-**1** (black), (*S,S*)-**3** (dark green) and (*R,S*)-**3** (light green) in N₂-purged acetonitrile solutions. A) Fluorescence spectra ($\lambda_{\text{exc}} = 310$ nm) and B) triplet excited state decays at 420 nm ($\lambda_{\text{exc}} = 266$ nm). Inset shows the triplet-triplet absorption bands 2.9 μs after the laser pulse.

Expectedly, triplet formation in (*S,S*)- and (*R,S*)-**3** was much less effective than for (*S*)-**1** (Fig. 4B), which can be attributed to quenching of the singlet precursor. This is consistent with the low reactivity of **3** in oxygenated media (Fig. 2 middle), where the quantum yield of ¹O₂ would be very low. Here, no shortening of

the τ_T values was observed, indicating the absence of any intramolecular quenching of the NPX triplet excited state.

Finally, neither fluorescence nor laser flash photolysis measurements exhibited noticeable differences between the unreactive (*S,S*)- and (*R,S*)-**4** and the model compound (*S*)-**1** (Fig. S7 of ESI), indicating the lack of any excited state interaction.

3.3 Photoproduct analysis

The attention was focused on the NPX-His system as it showed the highest oxygen-mediated photoreactivity (Fig. 2, middle). It is generally accepted that photooxygenation of His involves reaction with singlet oxygen.¹⁴ The primary products are unstable bicyclic endoperoxides,³³ which break down to give the final products.

The photomixtures obtained with (*S,S*)-**2** were submitted to UPLC-MS-MS. This led to detection of the major photoproducts **2a** and **2b**; the attributed structures are shown in Fig. 5.

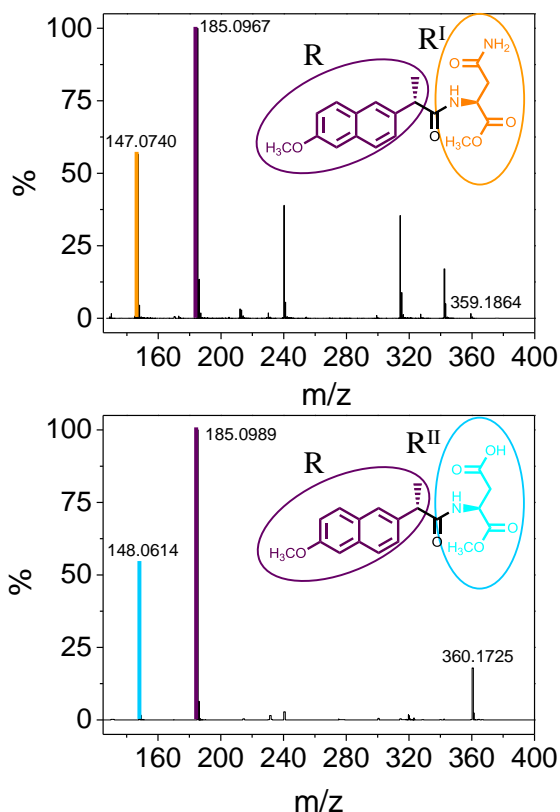


Fig. 5 Assigned structures and MS-MS spectra of the main photoproducts **2a** (top) and **2b** (bottom) obtained from (*S,S*)-**2**.

Structural assignment was based on the exact mass values, indicating molecular formulae $C_{19}H_{22}N_2O_5$ and $C_{19}H_{21}NO_6$. As regards the fragmentation patterns, both photoproducts shared a common naproxen-derived $C_{13}H_{13}O$ ion (denoted as R in Fig. 5), together with diagnostically important C_5 -fragments corresponding to the oxidation of His (R^I and R^{II} in Fig. 5).

Although the NPX-Trp systems reacted only sluggishly, UPLC-MS-MS analysis of the photolysates also revealed the

presence of typical Trp singlet oxygenation products^{5,34} in low amounts. Thus, Fig. 6 shows the MS-MS spectra tentatively assigned to the *N*-formylkynurenine **3a** (top) and 3-hydroxypyrrroloindole **3b** (bottom) derivatives. Exact mass determination led to the molecular formulae $C_{26}H_{26}N_2O_6$ and $C_{26}H_{26}N_2O_5$, respectively. The fragmentation patterns were fully consistent with this assignment.

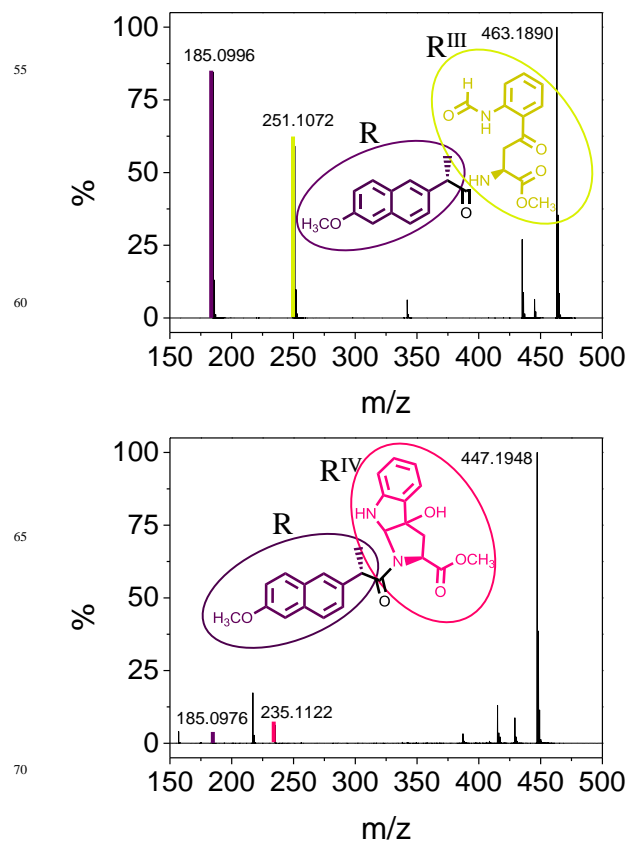


Fig. 6 Assigned structures and MS-MS spectra of the main photoproducts **3a** (top) and **3b** (bottom) obtained from (*S,S*)-**3**.

4 Conclusions

The photooxygenation mechanism of linked systems containing (*S*)- or (*R*)-naproxen and His, Trp or Tyr has been investigated by a combination of steady-state photolysis and photophysical measurements. The highest oxygen-mediated photoreactivity was observed for NPX-His, which gave rise to the aminosuccinic acid derivatives **2a** and **2b**, typical His-derived singlet oxygen products. Photodegradation was faster in air equilibrated than in fully oxygenated solutions, in agreement with the diminished production of $^3NPX^*$ -His under the latter conditions. The most remarkable feature of NPX-Trp systems was a fast and stereoselective intramolecular fluorescence quenching, which prevented efficient population of $^3NPX^*$ -Trp, thus resulting in a lower reactivity towards photooxygenation. However, analysis of the NPX-Trp photolysates by UPLC-MS-MS allowed detection of *N*-formylkynurenine **3a** and 3-hydroxypyrrroloindole **3b**, presumably arising from reaction of singlet oxygen (1O_2) with the

Trp moiety. Finally, the NPX-Tyr systems were nearly unreactive and exhibited photophysical properties essentially coincident with those of the parent NPX. Although other competing photoprocesses can in principle be envisaged (e. g. charge transfer quenching by Trp), the combined photophysical and photochemical results presented here point to the predominance of a type II photooxygenation mechanism, triggered by generation of $^1\text{O}_2$ from the triplet excited NPX chromophore. This reinforces the value of linked systems as models for non-covalent drug/protein complexes.

Acknowledgements

Financial support from the Spanish Government (CTQ2010-14882, JCI-2011-09926, Miguel Servet CP11/00154), from the EU (PCIG12-GA-2012-334257), from the Universitat Politècnica de València (SP20120757) and from the Consellería de Educació, Cultura i Esport (PROMETEOII/2013/005, GV/2013/051) is gratefully acknowledged.

Notes and references

Dedicated to the memory of Prof. Nicholas J. Turro.

^a *Departamento de Química/Instituto de Tecnología Química UPV-CSIC, Universitat Politècnica de València, Camino de Vera s/n, E-46022 Valencia, Spain. Tel. (+34)-963877344, Fax: (+34)-963879349. E-mail: mcjimene@qim.upv.es; mmiranda@qim.upv.es.*

^b *Unidad Mixta de Investigación IIS La Fe-UPV, Hospital La Fe, Avda. Campanar 21, 46009 Valencia, Spain.*

† Electronic Supplementary Information (ESI) available: additional X-ray structures, photodegradation kinetics, UV, fluorescence and transient absorption data (8 pages). See DOI: 10.1039/b000000x/

1. L. I. Grossweiner and K. C. Smith, *Photochemistry in The Science of Photobiology*, 2nd ed. (Smith, K. C., Ed.), Plenum Press, New York, 1989, pp 47-78.
2. L. Pretali and A. Albini, In *CRC Handbook of Organic Photochemistry and Photobiology*; 3rd ed., A. Griesbeck, M. Oelgemöller, F. Ghetti, Eds.; CRC Press: Boca Raton, FL, 2012; pp. 369-391.
3. C. S. Foote, Definition of type I and type II photosensitized oxidation, *Photochem. Photobiol.* 1991, **54**, 659.
4. K. Briviba, L. O. Klotz and H. Sies, Toxic and signaling effects of photochemically generated singlet oxygen in biological systems, *Biol. Chem.* 1997, **378**, 1259-1265.
5. M. J. Davies, Singlet oxygen-mediated damage to proteins and its consequences, *Biochem. Biophys. Res. Commun.* 2003, **305**, 761-770.
6. M. J. Davies, Reactive species formed on proteins exposed to singlet oxygen, *Photochem. Photobiol. Sci.* 2004, **3**, 17-25.
7. A. W. Girotti, Photosensitized oxidation of membrane lipids: reaction pathways, cytotoxic effects, and cytoprotective mechanisms, *J. Photochem. Photobiol. B* 2001, **63**, 103-113.
8. I. Andreu, I. M. Morera, F. Boscá, L. Sánchez, P. Camps and M. A. Miranda, Cholesterol-diaryl ketone stereoisomeric dyads as models for clean type I and type II photooxygenation mechanisms, *Org. Biomol. Chem.* 2008, **6**, 860-867.
9. E. R. Stadtman, Oxidation of free amino acids and amino acid residues in proteins by radiolysis and by metal-catalysed

reactions, *Annu. Rev. Biochem.* 1993, **62**, 797-821.

10. W. M. Garrison, Reaction mechanisms in the radiolysis of peptides, polypeptides and proteins, *Chem. Rev.* 1987, **87**, 381-398.
11. P. U. Giacomoni, Sun Protection in Man. *Comprehensive Series in Photosciences*, vol. 3. Elsevier: Amsterdam; 2001.
12. R. C. Straight and J. D. Spikes, Photosensitized oxidation of biomolecules. In: A. A. Frimer (ed.), O. Singlet (ed.). *Polymers and Biopolymers*, CRC Press: Boca Raton, FL, 1985: pp. 91-143.
13. A. Wright, W. A. Bubb, C. L. Hawkins and M. J. Davies, Singlet oxygen mediated protein oxidation: evidence for the formation of reactive side-chain peroxides on tyrosine residues, *Photochem. Photobiol.* 2002, **76**, 35-46.
14. V. V. Agon, W. A. Bubb, A. Wright, C. L. Hawkins and M. J. Davies, Sensitizer-mediated photooxidation of histidine residues: evidence for the formation of reactive side-chain peroxides, *Free Radical Biol. Med.* 2006, **40**, 698-710.
15. J. E. Huyett, P. E. Doan, R. Gurbiel, A. L. P. Houseman, M. Sivaraja, D. B. Goodin and B. M. Hoffman, Compound ES of cytochrome *c* peroxidase contains a Trp π -cation radical: characterization by CW and pulsed Q-band ENDOR spectroscopy, *J. Am. Chem. Soc.* 1995, **117**, 9033-9041.
16. R. W. Redmond and J. N. Gamlin, A compilation of singlet oxygen yields from biologically relevant molecules, *Photochem. Photobiol.*, 1999, **70**, 391-475.
17. A. J. Lewis and D. E. Furst, *Nonsteroidal Anti-Inflammatory Drugs: Mechanisms and Clinical Uses*, 2nd Edition; Marcel Dekker: New York, 1994.
18. F. Boscá, M. L. Marín and M. A. Miranda, Photoreactivity of the nonsteroidal anti-inflammatory 2-arylpropionic acids with photosensitizing side effects, *Photochem. Photobiol.* 2001, **74**, 637-655.
19. G. M. J. Beijersbergen van Henegouwen, Phototoxicity of drugs and other xenobiotics, *J. Photochem. Photobiol. B: Biol.* 1991, **10**, 183-210.
20. M. A. Miranda, J. V. Castell, D. Hernández, M. J. Gómez-Lechón, F. Boscá, I. M. Morera and Z. Sarabia. Drug-photosensitized protein modifications: identification of the reactive sites and elucidation of the reaction mechanisms with tiaprofenic acid/albumin as model system, *Chem. Res. Toxicol.*, 1998, **11**, 172-177.
21. M. C. Jiménez, U. Pischel and M. A. Miranda, Photoinduced processes in naproxen-based chiral dyads, *J. Photochem. Photobiol. C*, 2007, **8**, 128-142.
22. A. Catalfo, G. Bracchitta and G. de Guidi, Role of aromatic amino acid tryptophan UVA-photoproducts in the determination of drug photosensitization mechanism: a comparison between methylene blue and naproxen, *Photochem. Photobiol. Sci.*, 2009, **8**, 1467-1475.
23. I. Vayá, R. Pérez-Ruiz, V. Lhiaubet-Vallet, M. C. Jiménez and M. A. Miranda, Drug-protein interactions assessed by fluorescence measurements in the real complexes and in model dyads, *Chem. Phys. Lett.*, 2010, **486**, 147-153.
24. I. Vayá, M. C. Jiménez and M. A. Miranda, Excited state interactions in flurbiprofen-tryptophan dyads, *J. Phys. Chem. B*, 2007, **111**, 9363-9371.
25. I. Vayá, P. Bonancía, M. C. Jiménez, D. Markovitsi, T. Gustavsson and M. A. Miranda, Excited state interactions

-
- between flurbiprofen and tryptophan in drug-protein complexes and in model dyads. Fluorescence studies from the femtosecond to the nanosecond time domains, *Phys. Chem. Chem. Phys.*, 2013, **15**, 4727-4734.
- 5 26. A. G. Griesbeck, J. Neudörfl and A. de Kiff, Photoinduced electron-transfer chemistry of the bielectrophoric N-phthaloyl derivatives of the amino acids tyrosine, histidine and tryptophan, *Beilstein J. Org. Chem.*, 2011, **7**, 518-524.
27. B. Giese, M. Wang, J. Gao, M. Stoltz, P. Müller and M. Graber, Electron relay race in peptides, *J. Org. Chem.*, 2009, **74**, 3621-3625.
- 10 28. M. Cordes, A. Köttgen, C. Jasper, O. Jacques, H. Boudebous and B. Giese, Influence of amino acid side chains on long-distance electron transfer in peptides: electron hopping via “stepping stones”, *Angew. Chem., Int. Ed.* 2008, **47**, 3461-3463.
- 15 29. B. Abraham and L. A. Kelly, Photooxidation of amino acids and proteins mediated by novel 1,8-naphthalimide derivatives, *J. Phys. Chem. B*, 2003, **107**, 12534-12541.
30. E. Cadenas, Biochemistry of oxygen toxicity, *Annu. Rev. Biochem.*, 1989, **58**, 79-110.
- 20 31. D. de la Peña, C. Martí, S. Nonell, L. A. Martínez and M. A. Miranda, Time-resolved near infrared studies on singlet oxygen production by the photosensitizing 2-arylpropionic acids, *Photochem. Photobiol.*, 1997, **65**, 828-832.
- 25 32. B. A. Kerwin and R. L. Remmele, Protect from light: photodegradation and protein biologics, *J. Pharm. Sci.*, 2007, **96**, 1468-1479.
33. P. Kang and C. S. Foote, Synthesis of a C-13, N-15 labeled imidazole and characterization of the 2,5-endoperoxide and its decomposition, *Tetrahedron Lett.*, 2000, **41**, 9623-9626.
- 30 34. I. Saito, T. Matsuura, M. Nakagawa and T. Hino, Peroxidic intermediates in photosensitized oxygenation of tryptophan derivatives, *Acc. Chem. Res.*, 1977, **10**, 346-352.